The Hydrometeorology of Extreme Floods in the Lower Mississippi River

Yibing Su[a], James A. Smith,[a] and Gabriele Villarini[b]

[a] *Department of Civil and Environmental Engineering, Princeton University, Princeton, New Jersey*
[b] *IIHR—Hydroscience and Engineering, University of Iowa, Iowa City, Iowa*

ABSTRACT: The Lower Mississippi River has experienced a cluster of extreme floods during the past two decades. The Bonnet Carré spillway, which is located on the Mississippi River immediately upstream of New Orleans, has been operated 15 times since its completion in 1931, with 7 occurrences after 2008. In this study, we examine rainfall and atmospheric water balance components associated with Lower Mississippi River flooding in 2008, 2011, and 2015–19. We focus on multiple time scales—1, 3, 7, and 14 days—reflecting contributions from individual storm systems and the aggregate contributions from a sequence of storm systems. Atmospheric water balance variables—integrated water vapor flux (IVT) and precipitable water—are central to our assessment of the storm environment for Lower Mississippi flood events. We find anomalously large IVT corridors accompany the critical periods of heavy rainfall and are organized in southwest–northeast orientation over the Mississippi domain. Atmospheric rivers play an important role as agents of extremes in water vapor flux and rainfall. We conduct climatological analyses of IVT and precipitable water extremes across the four time scales using 40 years of North American Regional Reanalysis (NARR) fields from 1979 to 2018. We find significant increasing trends in both variables at all time scales. Increases in IVT especially cover large regions of the Mississippi domain. The findings point to increased vulnerability faced by the Mississippi flood control system in the current and future climate.

KEYWORDS: Hydrometeorology; Mesoscale processes; Water budget/balance

1. Introduction

The Mississippi River has experienced destructive floods throughout history. The most notable example—the Great Mississippi Flood of 1927—resulted in the development and construction of an elaborate flood control system (Lott and Myers 1956; Myers 1959; Barry 1997; Camillo 2012; Smith and Baeck 2015; Munoz et al. 2018). The Mississippi River is now regulated by a network of levees along its main channels, flood control dams and reservoirs on upstream tributaries, and spillways with outlet structures on the main channel of the Lower Mississippi. The system is designed to protect the region against extreme flooding in the Lower Mississippi up to a peak discharge of 3 million cfs (cubic feet per second). During extreme flood periods, spillways are operated to provide outlets that remove water from the main channel and deliver water to the Gulf of Mexico through alternate flow paths.

The most downstream spillway on the Lower Mississippi River is the Bonnet Carré Spillway (30°N, 90.44°W), which is located in St. Charles Parish, Louisiana, about 19 km west of New Orleans. The spillway takes advantage of a natural flow path created by the 1871 Bonnet Carré Crevasse and diverts water into Lake Pontchartrain and subsequently the Gulf of Mexico. It is designed to transport as much as 250 000 cfs from the river and is the last line of defense for New Orleans. Since its completion in 1931, the Bonnet Carré spillway has been activated 15 times. Operation of Bonnet Carré provides a useful index for significant flood events in the Lower Mississippi.

The first Bonnet Carré operation during the twenty-first century occurred in 2008, a gap of 11 years since the previous operation in 1997. Since 2008, Bonnet Carré has been operated 7 times, or roughly once every other year, a notable change from the 1-in-10-yr regime which held for almost 8 decades. In 2019, Bonnet Carré was operated twice for the first time in a single year. 2019 also marked the first time the spillway was operated in consecutive years. Flooding during 2020 resulted in the third consecutive year of operation. These twenty-first-century Bonnet Carré events comprise a cluster of high values in the annual maximum discharge record at Vicksburg, Mississippi (Fig. 1).

The increased frequency of spillway operation at Bonnet Carré raises the question of whether the frequency of extreme floods is increasing in the Lower Mississippi River and whether the 3 000 000 cfs criterion used for the design of the flood control system remains adequate (Munoz and Dee 2017; Van der Wiel et al. 2018; Munoz et al. 2018). In this study, we examine extreme rainfall events that result in Lower Mississippi flooding, focusing on events that have occurred since 2008, namely, the floods of 2008, 2011, and 2015–19. Among the six events, the 2017 flood was the only one that did not trigger operation of the Bonnet Carré spillway; distinctive features of the 2017 flood (as detailed below) played a role in flood control operations for the event. Analyses of these major flood episodes are used to guide assessments of non-stationarities in atmospheric water balance components that drive extreme rainfall.

A central objective of this study is to characterize and quantify the spatial and temporal properties of heavy rainfall which result in extreme Lower Mississippi River flood episodes. We use Stage-IV radar rainfall fields (Lin and Mitchell 2005; Du 2011) to examine rainfall variability over time scales

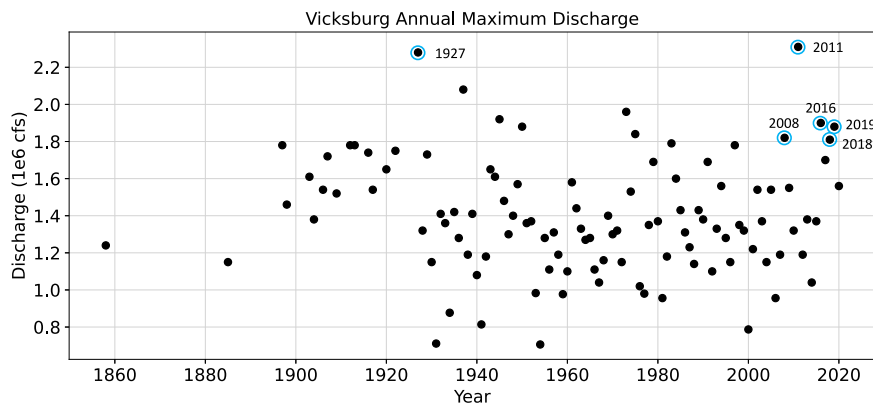*Corresponding author*: Yibing Su, yibings@princeton.edu

Fig. 1. Annual maximum flood peaks (cfs) for the Mississippi River at Vicksburg, Mississippi, from 1858 to 2019.

ranging from subdaily to multiple months. The longest time scale focuses on the two-month window preceding the time of peak discharge at the Vicksburg, Mississippi, U.S. Geological Survey (USGS) station.

In their innovative hydrometeorological studies of Lower Mississippi River flooding, Lott and Myers (1956) and Myers (1959) note that sequences of storms—often associated with powerful winter/spring extratropical cyclones—dictate the nature and magnitudes of Mississippi River floods (see also Smith and Baeck 2015). Indeed the number and sequencing of these storms is a key element of the resulting design storm—"Hypo-Flood 58a" (Lott and Myers 1956)—and a focus of this study.

Strong corridors of water vapor flux accompany the winter/spring storm systems that contribute to major floods in the Lower Mississippi River. Myers (1959) and subsequent studies (e.g., Dirmeyer and Kinter 2010; Lavers and Villarini 2013; Smith and Baeck 2015) have pointed to a close linkage between heavy rainfall and elevated atmospheric vapor transport in the main flood development region of the Lower Mississippi Valley. The moisture transport corridors in the Mississippi River basin are often strong enough and long enough to qualify as atmospheric rivers (as detailed below). In the AMS Glossary, an atmospheric river (AR) is defined as "a long, narrow, and transient corridor of strong horizontal water vapor transport that is typically associated with a low-level jet stream ahead of the cold front of an extratropical cyclone" (see Newell et al. 1992; Zhu and Newell 1998, for early analyses) for early analyses). ARs have been extensively studied as agents of extreme flooding along the West Coast of the United States (e.g., Ralph et al. 2006; Neiman et al. 2008; Ralph et al. 2019); less attention has been given to ARs and flooding east of the Rocky Mountains (e.g., Mahoney et al. 2016; Moore et al. 2012, 2015; Jennrich et al. 2020).

Flooding in the Lower Mississippi is affected by land surface processes and geomorphic processes that have changed over decades and centuries in response to both human activities and natural variability in the fluvial and climate system (Bentley et al. 2016; Munoz and Dee 2017; Russell et al. 2021; Wu et al. 2022; Wiman et al. 2021). Soil moisture, snow, and snowmelt can contribute to antecedent conditions that

modulate the hydrologic response of the watershed to rainfall extremes (Chen and Kumar 2002; Van der Wiel et al. 2018; Munoz and Dee 2017).

From an atmospheric water balance perspective (section 2), extreme rainfall is controlled by the convergence of atmospheric water vapor. Consequently, the vertically integrated water vapor flux field plays a central role in dictating extreme rainfall properties. We use the magnitude of the vertically integrated water vapor flux (IVT) as a key hydrometeorological variable for assessing extreme rainfall characteristics in the Lower Mississippi basin.

Precipitable water, the storage term in the atmospheric water balance, has played an outsized role in guiding engineering design (World Meteorological Organization 2009). The practice of upscaling environmental moisture availability to maximize precipitation has focused attention on precipitable water. For the Lower Mississippi River flood periods we compare anomalies in water vapor flux and precipitable water.

Su and Smith (2021) introduce a method for assessing hydrometeorological anomalies using climatology fields of IVT and precipitable water derived from North American Regional Reanalysis (NARR) fields (see also Hart and Grumm 2001). Here we employ similar methods to assess the 1–14-day IVT and precipitable water anomalies, which are the ratios of maximum n-day mean precipitable water and IVT with the n-day 10-yr return period fields. The anomaly analyses provide insight into the environmental controls of extreme rainfall and motivate analyses of non-stationarities in atmospheric water balance components. Recent studies have demonstrated the utility of atmospheric water balance analyses for examining the climatology of extreme rainfall (see e.g., Kunkel et al. 2020a,b).

We adopt an atmospheric water balance framework to investigate long-term trends in the hydrometeorological variables associated with Lower Mississippi River floods. Instead of directly examining non-stationarities in discharge extremes on the heavily regulated river, we assess trends in water vapor flux and precipitable water derived from reanalysis fields.

The paper is organized as follows. Data and methods are introduced in section 2. In section 3, we examine the hydrometeorology of extreme floods in the Lower Mississippi River
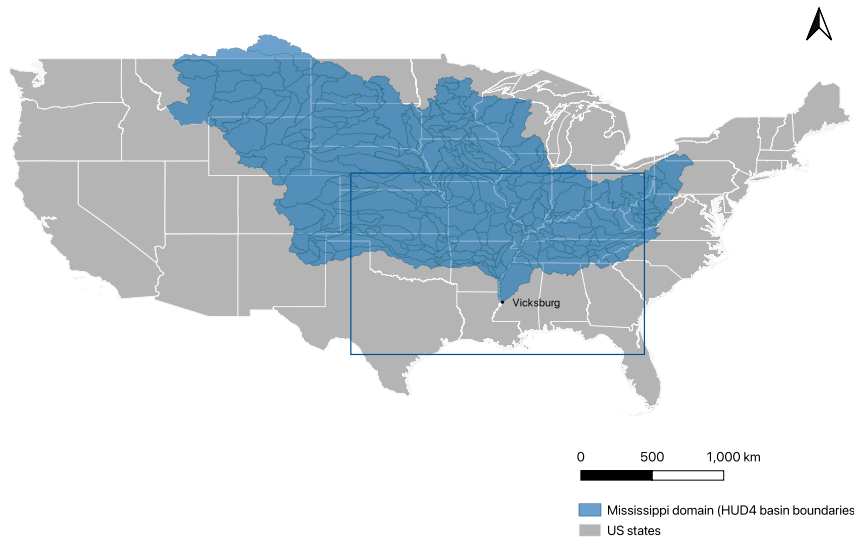
FIG. 2. Map of the Mississippi study domain. Blue polygons are the HUC 4 basins that make up the Mississippi study domain, defined as the Mississippi River drainage region upstream of Vicksburg, Mississippi. Gray polygons are the U.S. states. The black dot marks the location of the Vicksburg, Mississippi, USGS station, located at 32°18′54″N latitude, 90°54′21″W longitude. The blue box indicates the (81°–101°W, 29°–41°N) box region for which water balance variables are computed.

since 2008, principally through analyses of radar rainfall fields and atmospheric water balance components. Non-stationarities of the atmospheric water balance variables are examined in section 4, followed by the summary and conclusions in section 5.

2. Data and methods

For rainfall analyses, we use the National Centers for Environmental Prediction (NCEP) Stage-IV radar rainfall fields, which have hourly time scale and approximately 4-km spatial resolution (Lin and Mitchell 2005). Daily discharge measurements from the U.S. Geological Survey (USGS) stream gauging station on the Mississippi River at Vicksburg, Mississippi, are used for analyses of hydrologic response during the major flood episodes since 2008 and for analyses of annual flood peaks in the Lower Mississippi River.

Rainfall analyses are carried out for the drainage basin above Vicksburg (Fig. 2), which has an area of 2 976 000 km². The domain does not include the Red River tributary, which drains through the Atchafalaya River into the Gulf of Mexico. The Bonnet Carré spillway is downstream of the Mississippi River from Vicksburg (Fig. 2). Shapefiles for basin delineation
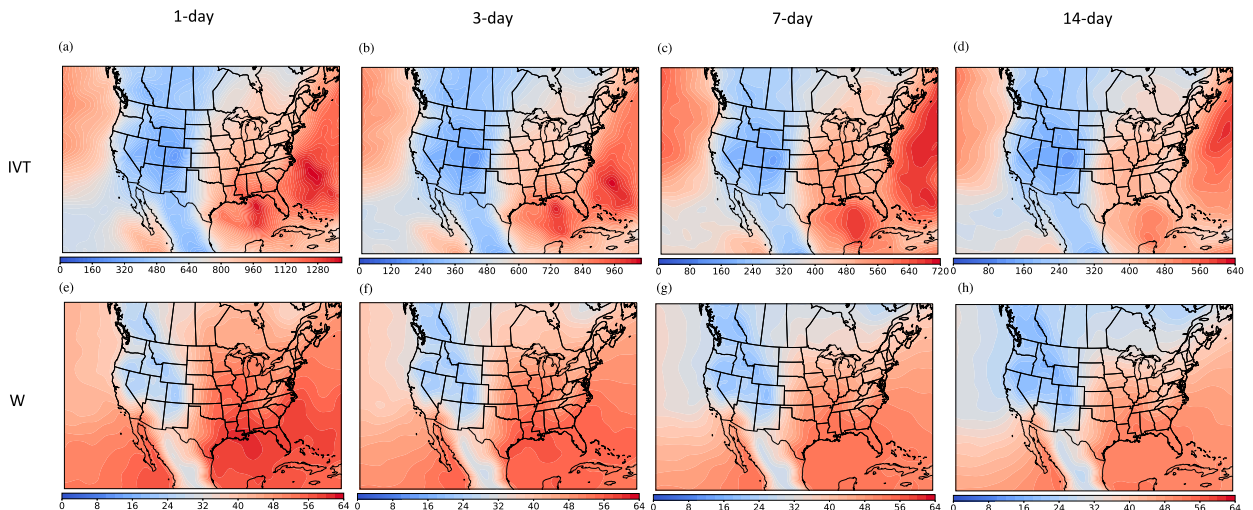

FIG. 3. The 10-yr return period fields for 1-, 3-, 7-, and 14-day (a)–(d) IVT (kg m^{-1} s^{-1}) and (e)–(h) precipitable water (mm).

TABLE 1. The *n*-day time windows with maximum average IVT over the box domain of (81°–101°W, 29°–41°N) during the six flood episodes.

	2008 24 Feb–24 Apr	2011 19 Mar–18 May	2015/16 15 Nov–14 Jan	2017 26 Mar–25 May	2018 15 Jan–16 Mar	2019 13 Jan–14 Mar
1-day window start time	1000 UTC 18 Mar 2008	0000 UTC 27 Apr 2011	0000 UTC 27 Dec 2015	1600 UTC 29 Apr 2017	2000 UTC 20 Feb 2018	0600 UTC 13 Feb 2019
3-day window start time	0800 UTC 17 Mar 2008	1000 UTC 25 Apr 2011	1100 UTC 26 Dec 2015	0000 UTC 29 Apr 2017	1400 UTC 19 Feb 2018	1600 UTC 10 Feb 2019
7-day window start time	0600 UTC 4 Apr 2008	1400 UTC 21 Apr 2011	0600 UTC 22 Dec 2015	1600 UTC 28 Apr 2017	1200 UTC 19 Feb 2018	1500 UTC 17 Feb 2019
14-day window start time	1300 UTC 29 Mar 2008	1600 UTC 14 Apr 2011	0400 UTC 21 Dec 2015	1300 UTC 21 Apr 2017	0100 UTC 16 Feb 2018	1500 UTC 10 Feb 2019

were obtained from the Hydrological data and maps based on the Shuttle Elevation Derivatives at multiple Scales (Hydro-SHEDS) mapping product (Lehner et al. 2008).

To characterize the spatial and temporal variability of rain over the Mississippi watershed we examine: 1) daily time series of basin area with rainfall exceeding 50 mm (denoted mm day^{-1}) for the 60 days prior to the peak discharge at Vicksburg; 2) hourly time series of basin area with rainfall exceeding 25 mm h^{-1} for the maximum 3-day rainfall period; 3) rainfall accumulation maps for the maximum 3-day rainfall period; 4) rainfall-weighted flow distance (RWFD) and dispersion for the maximum 3-day rainfall period over the basin above Vicksburg. The maximum 3-day rainfall period is selected as the period containing the largest rainfall accumulation during the 60-day window prior to the Vicksburg discharge peak.

The time series of area with daily rainfall greater than 50 mm day^{-1} provides a simple characterization of the storm sequencing leading to peak discharge at Vicksburg. We choose hourly rainfall rates of 25 mm h^{-1} as an index for distinguishing convective rainfall from stratiform rainfall (Steiner and Smith 1998). The basin area with rainfall exceeding 25 mm h^{-1} provides a measure of the convective rainfall extent over the Mississippi domain. Rainfall accumulation maps for the maximum 3-day rainfall period illustrate the spatial structure of rainfall associated with the most extreme storm episode.
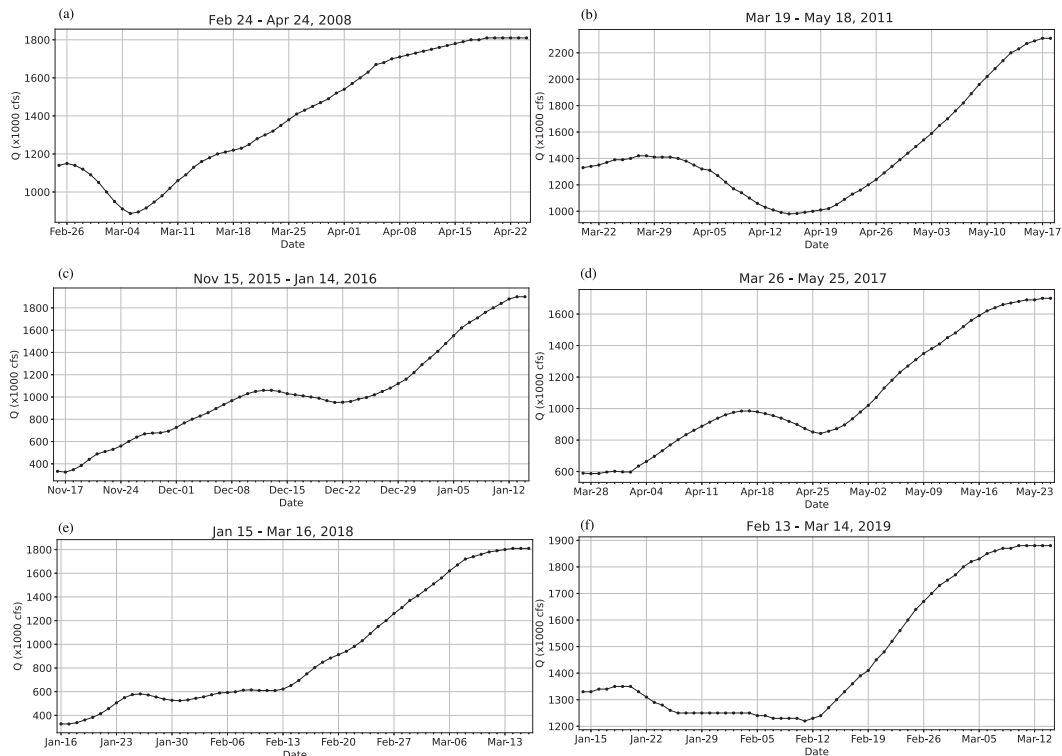

FIG. 4. Time series of daily discharge (cfs) of the Mississippi River at Vicksburg for the 60 days preceding Vicksburg peak discharge on (a) 24 Apr 2008, (b) 18 May 2011, (c) 14 Jan 2016, (d) 25 May 2017, (e) 16 Mar 2018, and (f) 14 Mar 2019.

FIG. 5. Daily Lower Mississippi basin area (km^2) with rainfall exceeding 50 mm for the 60 days preceding Vicksburg peak discharge on (a) 24 Apr 2008, (b) 18 May 2011, (c) 14 Jan 2016, (d) 25 May 2017, (e) 16 Mar 2018, and (f) 14 Mar 2019. Note that the vertical axes differ for each event.
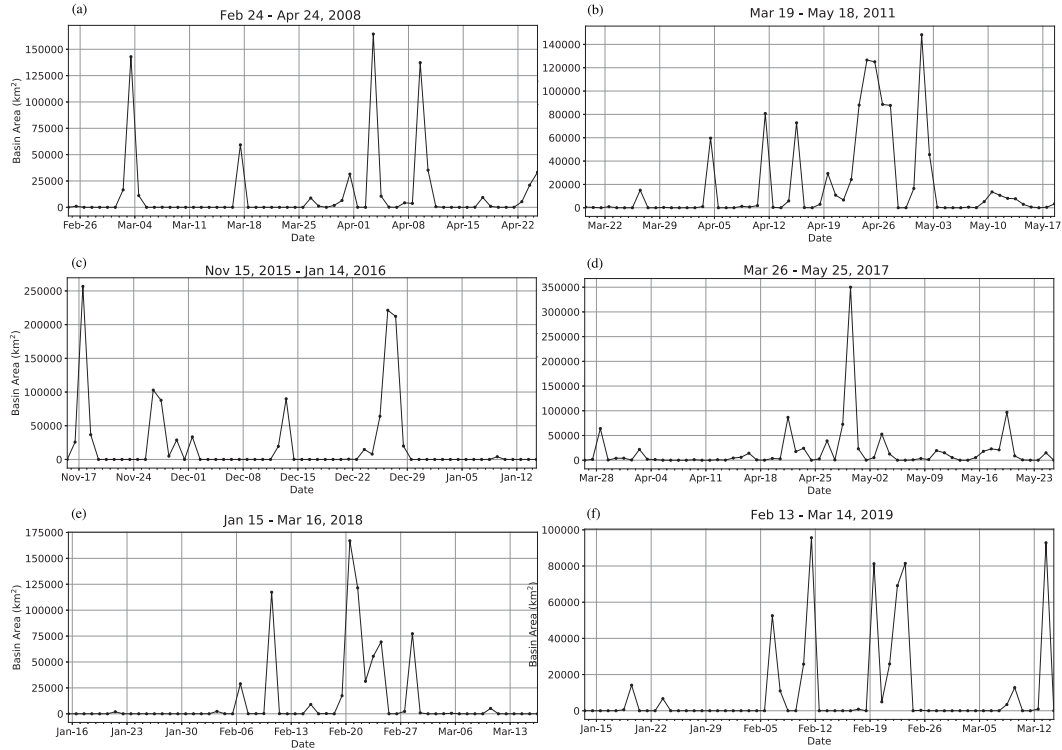
The rainfall-weighted flow distance D (Smith et al. 2002, 2005) for any n-day period is a function of the rainfall field $R(x)$ accumulated over the n days, and the distance function $d(x)$ that represents the flow distance from location x through the drainage network to the basin outlet:

$$D = \int_A w(y)d(y)dy, \qquad (1)$$

where A is the Lower Mississippi domain, $d(x)$ (km) is the flow distance along the drainage network from location x within the basin to the outlet at the USGS Vicksburg station. The "weight" for location x, $w(x)$, is given by the ratio of the rainfall at x, $R(x)$ (mm), to the mean rainfall over the domain:

$$w(x) = \frac{R(x)}{\int_A R(y)dy}. \qquad (2)$$

The *atmospheric water balance equation* represents time changes in precipitable water as additions from surface evaporation, losses from precipitation to the surface and water vapor convergence:

$$\frac{\partial W}{\partial t} = E - P - 3600\nabla \cdot \mathbf{Q}, \ (\text{mm h}^{-1}), \qquad (3)$$

where P is the precipitation rate (mm h^{-1}), E is the evaporation rate (mm h^{-1}), and W is the precipitable water (mm):

$$W = \int_0^{z_t} \rho_v(z)dz, \qquad (4)$$

where z_t denotes the elevation of the top of the troposphere and $\rho_v(z)$ (kg m^{-3}) is the mass of water vapor per unit volume of atmosphere at elevation z. The vertically integrated water vapor flux vector $\mathbf{Q} = (Q_x, Q_y)$, is defined as follows:

$$Q_x = \int_0^{z_t} \rho_v(z)u(z)dz, \qquad (5)$$

$$Q_y = \int_0^{z_t} \rho_v(z)v(z)dz, \qquad (6)$$

where $u(z)$ is the east–west component of the wind (m s^{-1}; positive eastward) at elevation z, and $v(z)$ is the north–south component of the wind (m s^{-1}; positive northward) at elevation z.

We compute zonal and meridional water vapor transport components using the 3-hourly 0.3° resolution specific humidity, wind, surface pressure and height fields from the North American Regional Reanalysis (NARR; Mesinger et al. 2006). NARR is a dynamically consistent product with temporally continuous fields for the North America starting at the beginning of 1979. We compute IVT (kg m^{-1} s^{-1}) as the magnitude of the zonal and meridional water vapor transport:

$$\text{IVT} = (Q_x^2 + Q_y^2)^{1/2}. \qquad (7)$$

TABLE 2. Number of days that Vicksburg discharge exceeded specified thresholds during the six flood episodes. Total count periods include 60 days prior to and 30 days after the Vicksburg peaks.

Date	>1 000 000 cfs	>1 250 000 cfs	>1 500 000 cfs	>1 750 000 cfs	>2 000 000 cfs
2008	82	48	31	15	0
2011	85	66	36	26	17
2015/16	45	28	20	11	0
2017	47	35	20	0	0
2018	52	32	22	10	0
2019	90	71	46	29	0

Su and Smith (2021) introduce a method for assessing atmospheric moisture anomalies using 10-yr return period fields computed from 40 years of 3-hourly NARR fields. We adopt similar methods in this study to compute the 10-yr return period fields of the 1-, 3-, 7-, and 14-day mean IVT and precipitable water, which serve as the basis of comparison for heavy rainfall periods of interest. We compute the 1-, 3-, 7-, and 14-day mean fields for the two variables across the continental United States (CONUS) for moving n-day windows from 1979 to 2018. We then extract annual maxima of the n-day mean, from which we compute the 90th percentile—10-yr return period—fields for each of the time scales. As in Su and Smith (2021), we employ a regionalization method through spatial smoothing of fields using a Gaussian filter from the open-source computing library SciPy (Virtanen et al. 2020); a smoothing window width of 3 is used. The 10-yr return period fields for n-day IVT and precipitable water (Fig. 3) exhibit large spatial variability with the central and eastern United States experiencing the highest precipitable water and IVT values across the CONUS. Precipitable water values also tend to be higher toward the Gulf Coast.

For each of the six flood episodes in 2008, 2011, and 2015–19, we compute the running n-day average atmospheric water balance variables over a boxed region of (81°–101°W, 29°–41°N), which centers on the Lower Mississippi, for the 60 days prior to the Vicksburg discharge peak. From these we extract one window with the highest domain-average IVT for each time scale. The resulting time windows, shown in Table 1, are periods we focus on for analyses of rainfall and atmospheric water balance variables patterns. We compare the precipitable water and IVT values from these n-day windows with the 10-yr n-day precipitable water IVT fields to arrive at the anomaly assessments of the atmospheric water balance variables during the flood episodes of 2008, 2011, and 2015–19.

Using the 40 years of NARR fields, we assess the presence of monotonic trends in the annual maxima of 1-, 3-, 7-, and 14-day mean IVT, precipitable water, and precipitable water during maximum IVT periods. We use the Mann–Kendall test for monotonic trends (Helsel and Hirsch 1993). The p value statistic is the principal tool for the assessment of significant trends and corresponds to the detected significance level of the null hypothesis. Additionally, we compute the Sen's slope estimator (Helsel and Hirsch 1993) to reflect the sign and magnitude of trends in the time series. We perform both the Mann–Kendall test and the Sen's slope estimation in R Core Team using the freely available trend package (Pohlert 2018).

To examine storm sequencing, we apply an atmospheric river (AR) detection algorithm to Twentieth Century Reanalysis, version 3 fields (20CRV3) to identify the series of ARs preceding Vicksburg flow peaks (Compo et al. 2011). 20CRV3 is a 1° and 3-hourly resolution dynamically consistent product with temporally continuous fields over the globe starting at the beginning of 1836 (Compo et al. 2006, 2011; Slivinski et al. 2019). We use IVT as the primary metric to identify ARs, adopting the algorithm developed in Lavers and Villarini (2013) and later modified in Nayak and Villarini (2017). Each AR has a continuous region—longer than 1000 km—of IVT exceeding 500 kg m^{-1} s^{-1}, and a duration of no less than 18 h. We search IVT fields from 34° to 45°N, over the longitude band from 100° to 70°W. Each identified AR is tracked down to 20°N and up to 57°N. The domain from 20°–57°N to 100°–70°W provides a focus on ARs that impact the Mississippi River basin. We use Twentieth Century Reanalysis fields for AR detection based on previous analyses of extreme floods in the Lower Mississippi River over the past century (Smith and Baeck 2015); future studies will assess the climatology of ARs drawing on the long record from the Twentieth Century Reanalysis.

3. Hydrometeorology of Lower Mississippi River floods: 2008–19

The sequence of flood episodes triggering operation of the Bonnet Carré Spillway form a cluster of high flow events in
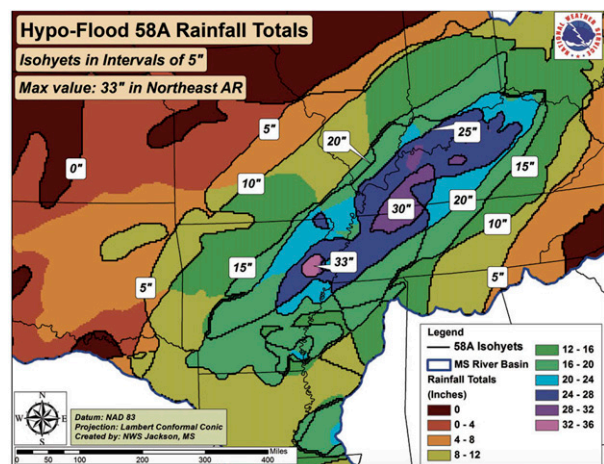

FIG. 6. Storm total rainfall for the design storm, HypoFlood-58a for the Lower Mississippi River flood control system (from NWS).
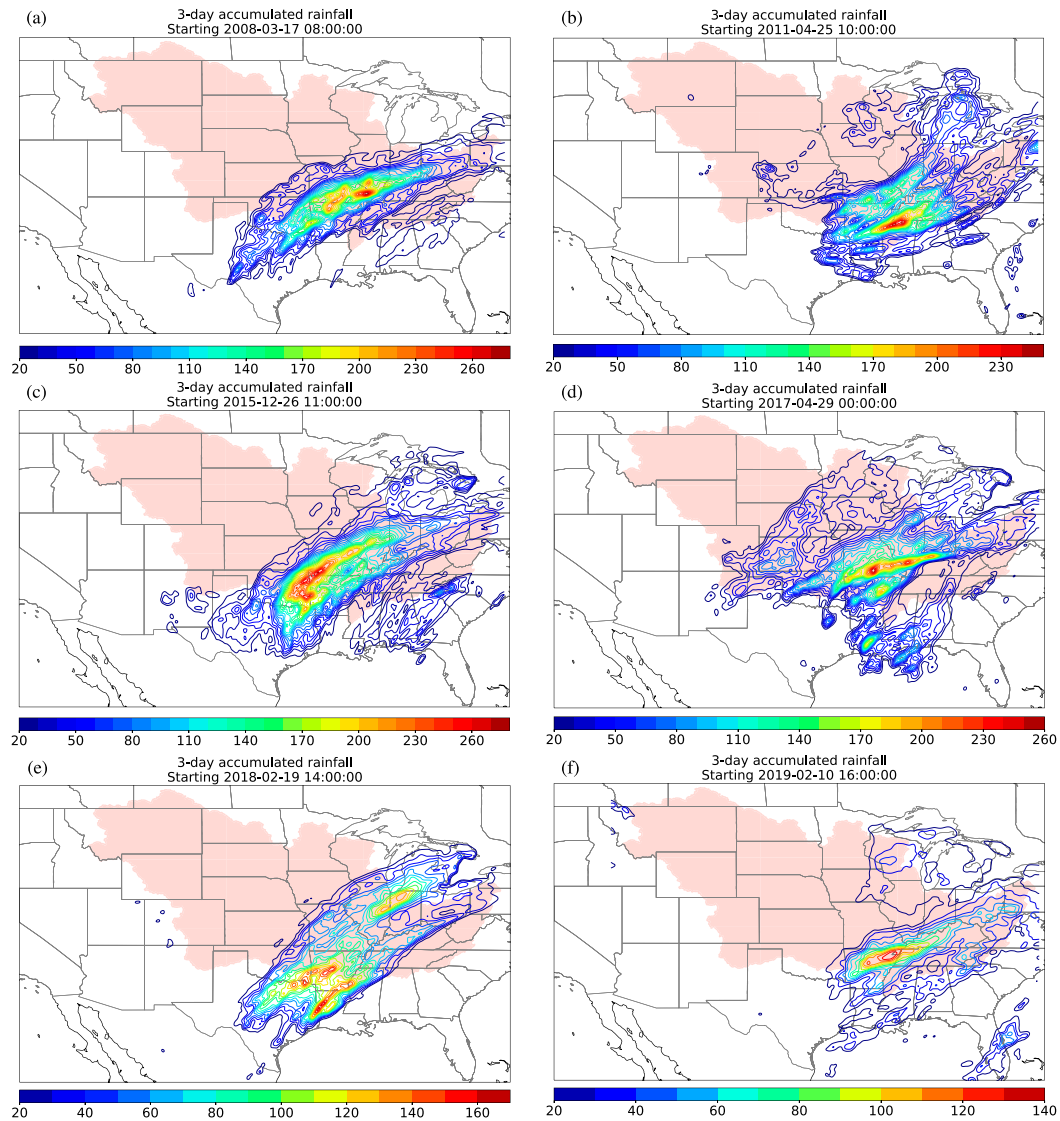
FIG. 7. Maximum 3-day rainfall (mm) for the six storms. The Mississippi River drainage domain upstream of Vicksburg is shaded in pink.

the annual maxima discharge time series for the Mississippi River station at Vicksburg, Mississippi (Fig. 1). The record flow at Vicksburg, 2 310 000 cfs was recorded during the 2011 flood. The second largest peak flow was recorded during the Great Flood of 1927.

Mississippi River floods come in different forms, largely tied to details of the sequence of storms that precede peak flooding. We illustrate the time-varying properties of extreme streamflow in the Lower Mississippi River through time series of discharge and rainfall exceedance area for the 60 days preceding peak discharge (Figs. 4 and 5). A summary of discharge values during the period 60 days prior to and 30 days after the peak discharge is given in Table 2.

Flood duration is a key element of the flood hazard in the Lower Mississippi River, especially in connection with levee safety (Camillo 2012). The 2011 flooding produced a peak

discharge greater than 2 000 000 cfs and 17 days with discharge greater than 2 000 000 cfs. Flooding during 2019 was most distinctive in duration of flooding, exceeding the 2011 episode in terms of the number of days exceeding 1 750 000 cfs. For all of the flood episodes, discharge exceeded 1 500 000 cfs for more than 20 days.

Lower Mississippi floods are dependent on rainfall over time scales ranging from subdaily to multiple months. Previous studies of Lower Mississippi rainfall extremes have pointed to the difficulty in understanding how storm systems are linked together to produce large rainfall accumulations over the same region for extended durations (Lott and Myers 1956; Myers 1959). Sequencing of storms associated with flooding along the West Coast of the United States has been examined in terms of "families" of ARs (Fish et al. 2019, 2022). For design of the Lower Mississippi River flood control system, a synthetic storm event—Hypo-Flood 58a (Fig. 6)—was

TABLE 3. Rainfall summaries for the maximum 3-day rainfall for prior to the floods of 2008, 2011, and 2015–19.

Date	RWFD (km)	RWFD dispersion (km)	Area > 100 mm (km^2)	Area > 200 mm (km^2)	Max rain (mm)	Basin average rain (mm)
2008	1110	870	216 000	25 300	320	22.4
2011	1180	940	186 000	10 600	310	23.8
2015/16	1100	860	317 000	57 800	340	28.7
2017	1339	800	222 000	24 000	310	32.4
2018	1200	910	79 100	—	191	19.6
2019	1170	740	40 840	—	153	15.0

constructed by stitching together rainfall from three major storms during January 1938, January 1950, and February 1937 (Camillo 2012). The time scale of rainfall for each storm was approximately 3 days and the storms were separated by 3 days; each of the heavy rainfall storms was associated with a powerful winter-season extratropical cyclone (Smith and Baeck 2015).

The basic patterns of rainfall organization in time and space embedded in HypoFlood 58-A are prominent features of the 2008–19 flood periods. Like the design storm components of HypoFlood 58-A, the twenty-first-century flood episodes in the Lower Mississippi are driven by storm systems producing extreme rainfall over 1–3-day time periods with a striking southwest to northeast organization (Fig. 7). The rainfall analyses in Fig. 7 are based on periods of maximum 3-day rainfall for each flood episode, which are the fundamental building blocks of HypoFlood 58a. The maximum accumulated rainfall in those 3-day episodes range from 153 mm in 2019 to 340 mm in 2015 (Table 3). The southwest–northeast orientation of extreme rainfall is similar over time periods ranging from 3 to 14 days (figures not shown).

Rainfall patterns for the six 3-day storm periods are not just visually similar, they are similar in properties that are central to flood response in the Lower Mississippi at Vicksburg—namely, the distribution of flow distances to the basin outlet. For the 2008, 2011, 2015, 2018, and 2019 events, the rainfall-weighted flow distance (RWFD) for the maximum 3-day rainfall (as in Fig. 7) ranges from 1100 to 1200 km. Values of RWFD dispersion—essentially the standard deviation of RWFD—range from 740 to 940 km, providing further quantitative grounding of the effects of storm structure on flood response (Table 3).

The 2017 flood episode is an outlier in terms of rainfall distribution, with an RWFD of 1340 km. The relatively large RWFD for this event extended the lead time for assessing

flood magnitudes in the Lower Mississippi, facilitating management of the flood without operation of Bonnet Carré. The relatively modest increase in rainfall weighted flow distance, associated with a more northerly distribution of rainfall, translates to significant differences in both flood response and flood management. The small spatial shift in rainfall distribution for the 2017 flood event relative to other storms resulted in larger contributions from the Missouri River, with significantly larger flow distances to Vicksburg. Distribution of rainfall relative to drainage network structure is central to rainfall-weighted flow distance and flood response in the Lower Mississippi.

Magnitudes of rainfall exhibit large variability for peak 3-day rainfall among the 6 flood episodes. The 24–26 December 2015 period produced rainfall accumulations exceeding 100 mm over an area of 317 000 km^2 in the Mississippi domain. For the 10–12 February 2019 period the area with rainfall greater than 100 mm was 40 800 km^2, almost an order of magnitude smaller than the maximum area for the 2015 storm. Peak 3-day rainfall accumulations for the 2011 flood included a maximum value of 310 mm and an area of 186 000 km^2 with rainfall exceeding

TABLE 4. Atmospheric rivers detected from March to mid-May 2011.

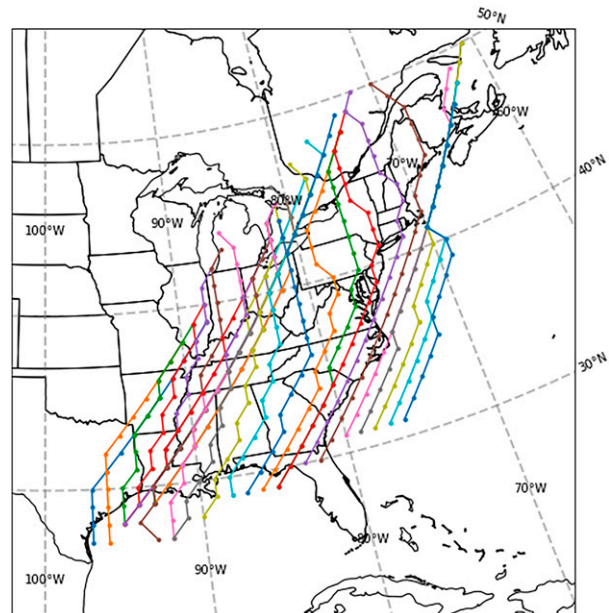| AR No. in 2011	Start time	Duration (h)
6	1800 UTC 6 Mar 2011	18
7	1800 UTC 8 Mar 2011	27
8	2100 UTC 10 Mar 2011	24
9	0000 UTC 4 Apr 2011	51
10	0000 UTC 10 Apr 2011	39
11	0900 UTC 15 Apr 2011	51
12	1800 UTC 25 Apr 2011	93
13	1800 UTC 30 Apr 2011	21
14	1800 UTC 11 May 2011	18

FIG. 8. Track map of an atmospheric river event from 1800 UTC 25 Apr to 1200 UTC 29 Apr 2011, as it propagates from west to east, detected using the Twentieth Century Reanalysis. Each connected dotted line represents the 3-hourly instantaneous position of the AR.
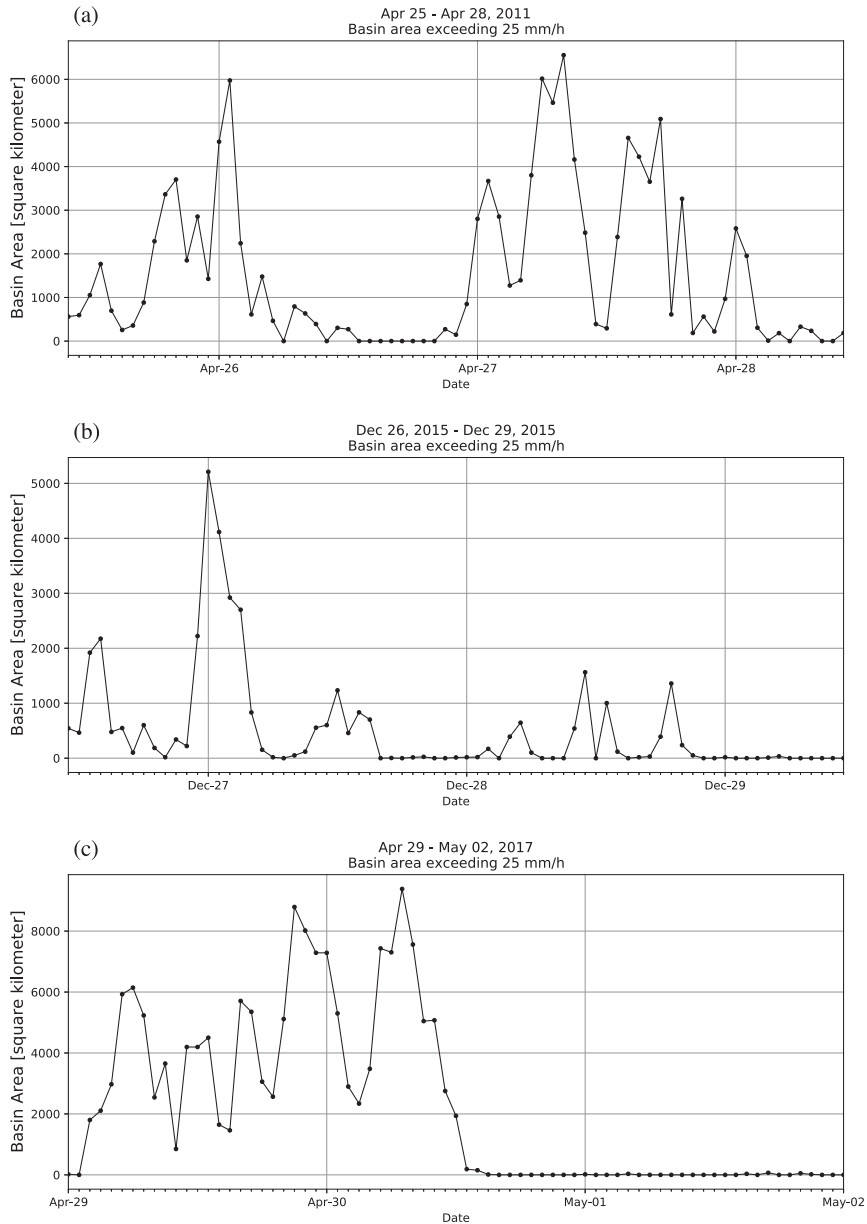
FIG. 9. Hourly Lower Mississippi basin area (km^2) with rainfall exceeding 25 mm for the 3-day maximum rainfall period of (a) 2011, (b) 2015, and (c) 2017.

100 mm. These values are smaller than the peak accumulations from 2008, 2015, and 2017. The area with rainfall exceeding 200 mm in 2011 falls even further behind the 2008, 2015, and 2017 values (Table 3).

Long-duration flooding in 2019 resulted from rainfall extremes over time scales longer than 2 months. Discharge at the beginning of the 60-day window preceding peak flow was greater than 1 300 000 cfs. A sequence of storms with modest rainfall accumulations (Fig. 7) produced flooding with the largest number of days exceeding all discharge thresholds above 1 000 000 cfs (Table 2). For the December–January

2016 and February–March 2018 flood events, discharge 60 days before the peak flow was less than 400 cfs, reflecting relatively dry conditions preceding this time window.

The 18 May 2011 flood peak in the Lower Mississippi River was generated by an exceptional sequence of winter/spring storms during the 3 months preceding the peak discharge. Flow of the Mississippi River at the beginning of the 60-day window preceding the flood peak was more than 1 300 000 cfs, following extreme rainfall during the preceding month (Fig. 4b). From the beginning of March to mid-May, we identified 9 separate atmospheric river episodes (Table 4)
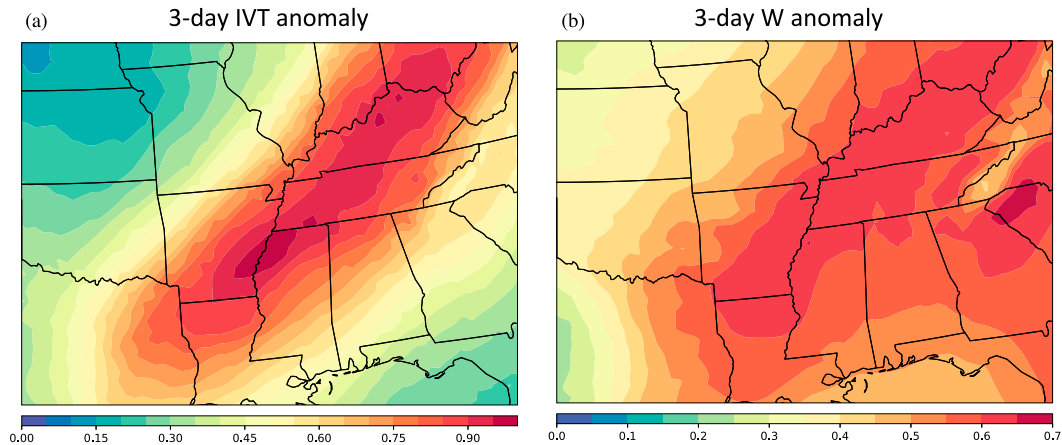
FIG. 10. Anomaly maps of 3-day (a) IVT and (b) precipitable water during maximum IVT from 25 to 27 Apr 2011.

that produced heavy rainfall over the watershed, beginning with the 6 March event that initiated a period of increasing flow at Vicksburg. ARs accompany the extreme rainfall episodes in all 6 events we investigate (figures not shown).

The most extreme rainfall preceding the 2011 flood peak (Fig. 5) was associated with an AR episode that extended from 25 to 29 April (Fig. 8). This AR event is the longest in duration leading up to Vicksburg flow peak. The AR originated in the central United States and moved eastward, with a southwest to northeast orientation over the Mississippi basin. It was associated with extreme rainfall and major tornado outbreaks; more than 200 tornadoes were reported on 27 April alone (https://www.spc.noaa.gov/exper/archive/events/). Clusters of supercell thunderstorms (Knupp et al. 2014) contributed to extreme convective rainfall and flooding in the Lower Mississippi (see Smith et al. 2001; Nielsen and Schumacher 2020, for discussion of supercells and extreme rainfall).

Extreme convective rainfall was central to record flooding in 2011, as it was for the Great Flood of 1927 (Smith and Baeck 2015); in Fig. 9a, we illustrate convective rainfall through time series of area with hourly rainfall rates exceeding

25 mm h^{-1} for the 3-day period with maximum rain. In Figs. 9b and 9c, we provide similar figures for December 2015 and April 2017, both with extreme convective rainfall. The April 2017 and December 2015 storms were also associated with tornado outbreaks, with 6 during the 25–26 December 2015 storm and 58 during the 28–30 April 2017 storm (https://www.spc. noaa.gov/exper/archive/events/).

Peak 1–3-day accumulations for the 2011, 2015–17 floods (Figs. 5 and 7) were tied to size and motion of extreme convective rainfall. For the 25–29 April 2011 storm period, convective rain area (represented by hourly rainfall rates greater than 25 mm h^{-1}) exceeds 2000 km^2 for 22 h. For the April 2017 storm there are 30 h with convective rain area exceeding 2000 km^2 and 36 consecutive hours of convective rain. For the December 2015 storm, convective rain area exceeds 2000 km^2 for 6 h.

Extreme rainfall in the Lower Mississippi River is paired with extremes in the atmospheric water balance, especially the vertically integrated water vapor flux (Figs. 10–13 and Tables 5 and 6). Peak values of IVT approach or exceed 10-yr return interval values for each of the six storms and for time
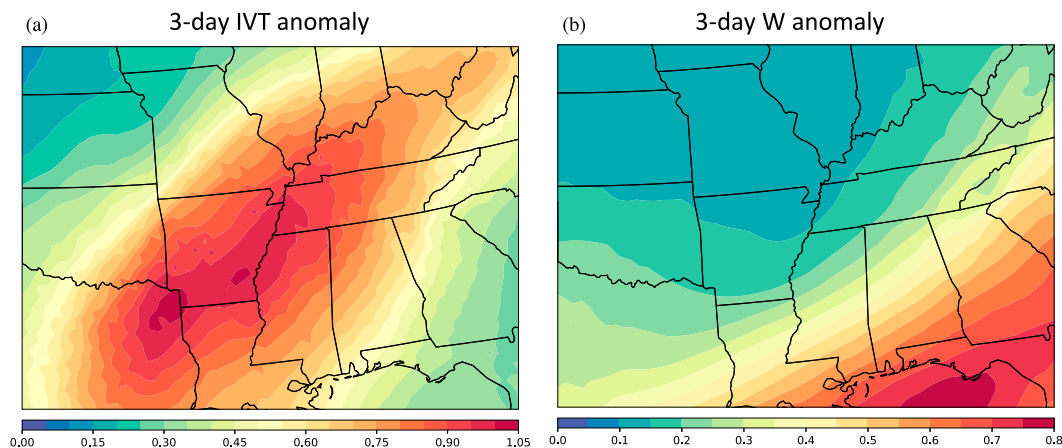

FIG. 11. Anomaly maps of 3-day (a) IVT and (b) precipitable water during maximum IVT from 26 to 28 Dec 2015.
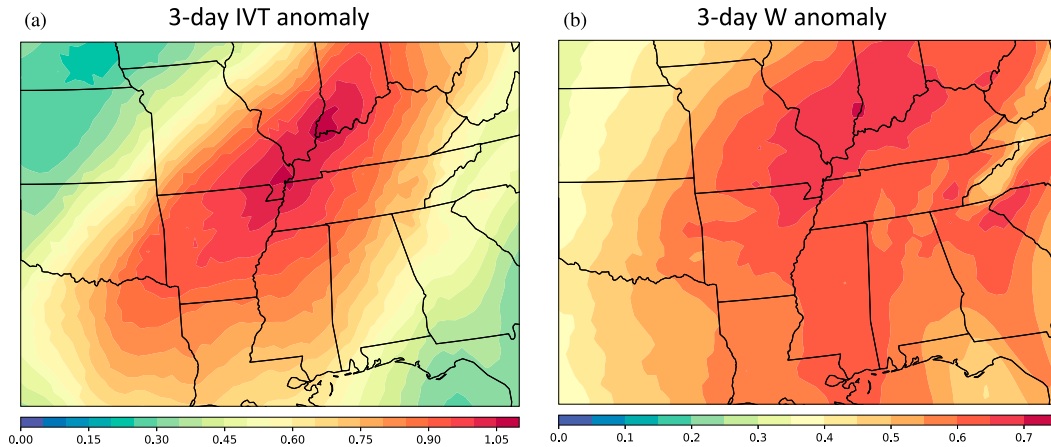
FIG. 12. Anomaly maps of 3-day (a) IVT and (b) precipitable water during maximum IVT from 29 Apr to 1 May 2017.

scales ranging from 1 to 14 days (Table 6); 10-yr return interval values correspond to normalized anomalies of 1. For precipitable water, peak values of normalized anomaly are significantly smaller, reflecting the primary role of water vapor flux for extreme rainfall. For the six flood episodes, extremes of precipitable water are large relative to seasonal norms, but small relative to the normalized IVT values.

Like the maximum 3-day rainfall accumulations, regions of highest IVT anomalies for all six flood episodes have a southwest–northeast orientation, which is similar for time scales ranging from 1 to 14 days. Figures 10–12 show 3-day anomaly fields for 2011, 2015, and 2017; Fig. 13 shows the 14-day anomaly field for 2011.

The absolute values of maximum IVT anomalies vary across the time scales and from event to event (Table 6). The largest normalized anomaly for IVT at 3-day time scale is 1.09 for the 2017 storm; the smallest is 0.88 for the 2008 storm. For the 2017 flood episode IVT anomalies are largest (1.09) at 3-day time scale and smallest (0.91) at 14 days. For the 2011 flood, IVT anomalies are largest at a 7- and 14-day time scale, 1.13 and 1.12, respectively.

Extreme rainfall and flooding in 2011 were tied to the exceptional area with anomalously large water vapor transport at time scales longer than 1 week. For the 2011 storm, the area with normalized anomalies values greater than 1 at the 14-day time scale (Fig. 13) was 404 000 km^2. At the 3-day time scale, the 2017 storm stands out for extremes in the area with anomalously large water vapor transport; normalized anomalies are greater than 1 over an area of more than 100 000 km^2 and exceed 0.85 over an area of more than 500 000 km^2 (Table 5). Zhang et al. (2019) examine the links between extreme water vapor transport in West Coast ARs and intensity of extratropical cyclones. Similar analyses could shed light on extremes of water vapor transport for storm periods that drive major flooding in the Lower Mississippi.

As illustrated in Fig. 5, there is a spectrum of storm sequences that produce major flooding in the Lower Mississippi River. Extreme rainfall is closely coupled with extremes of atmospheric water vapor flux over a range of time scales. In the following section, we explore changing climatology of extreme rainfall and flooding in the Lower Mississippi River through analyses of nonstationarities in extremes of the atmospheric water balance.
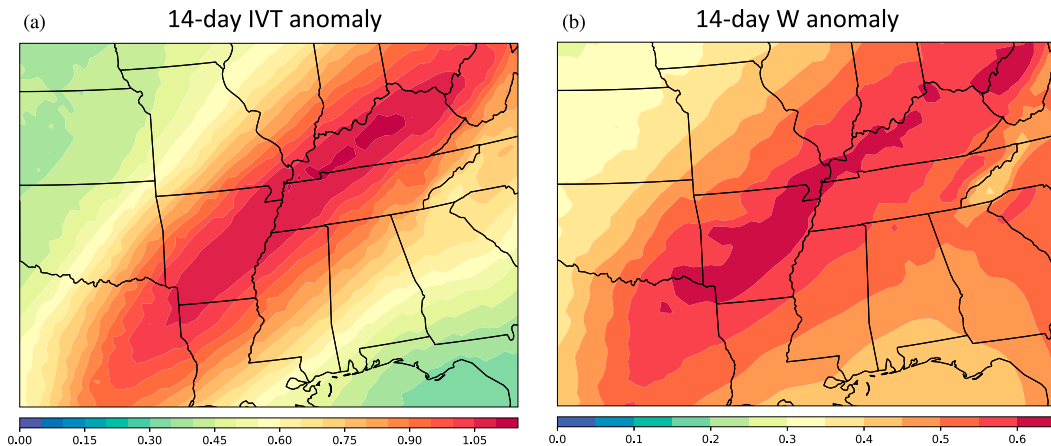

FIG. 13. Anomaly maps of 14-day (a) IVT and (b) precipitable water during maximum IVT from 14 to 27 Apr 2011.

TABLE 5. Mississippi domain area (km^2) with 3-day IVT anomalies over 0.85, 0.9, and 1 during the six flood episodes.

Anomaly thresholds	2008	2011	2015/16	2017	2018	2019
0.85	15 400	396 000	424 000	578 000	321 000	3070
0.9	—	211 000	286 000	413 000	145 000	—
1	—	—	19 500	103 000	1020	—

4. Extremes of the atmospheric water balance: Analyses of non-stationarities

As shown in the previous sections, pronounced anomalies in the atmospheric water balance are tied to long-duration heavy rainfall and flooding in the Lower Mississippi River. In this section, we investigate time trends in the extremes of n-day precipitable water and IVT, with a focus on the Mississippi domain; these analyses are used to infer changing properties of extreme rainfall and flood hazards in the region. Su and Smith (2021) conducted tests for abrupt changes on the 3-hourly precipitable water and IVT fields derived from NARR and found no significant evidence for these forms of non-stationarity in the annual maxima time series. In this study, we employ the Mann–Kendall test to examine monotonic trends in the 40-yr annual maxima of 1-, 3-, 7-, and 14-day average IVT, precipitable water, and precipitable water during maximum IVT time periods.

a. IVT

During the 40-yr period from 1979 to 2018, we found significant increasing trends in IVT over extensive areas of the Mississippi domain at all time scales (Fig. 14). At the 1-day time scale, the Mississippi domain is almost entirely within the region with 95% confidence level of monotonic increase (yellow lines in Fig. 14a). The strongest trends are located over the southeastern portion of the domain and reach 6.2 kg m^{-1} s^{-1} yr^{-1} on the daily scale (Figs. 14a,e). The upper Missouri River tributary has less significant evidence of increasing IVT. Significant trends with monotonic increase in IVT hold as time scale increases from 1 to 14 days, albeit with decreasing absolute values and spatial extent.

At the longest time scale—14 days—the region outlined by the 95% significance level over the Mississippi parses into two regions—one extending from the east coast of Texas and taking a southwest–northeast orientation over the lower and eastern portions of the Mississippi domain; the other one taking a south–north orientation over western portions of the domain. The swath of increasing IVT in the lower and eastern Mississippi resembles the Maya Express corridor, which is responsible for transporting anomalously large amounts of water vapor from the Gulf of Mexico into the Mississippi River basin. The average 14-day IVT increases at a maximum rate of 2.04 kg m^{-1} s^{-1} yr^{-1} over this swath, which is also the largest increase rate at the 14-day time scale over the CONUS. The location and orientation of this swath of increasing IVT coincide with the location and orientation of the anomalously large IVT fields during the events analyzed in section 3.

The evidence of increase in IVT across all time scales points to increasing heavy rainfall potential over most of the Mississippi domain—particularly regions that contribute to major floods in the Lower Mississippi. These increases in IVT point to heightened vulnerability of the Lower Mississippi flood control system.

Outside the Mississippi domain, the Mexican Plateau, the Columbia Plateau, and the North Atlantic basin are also experiencing increases in IVT. Increases in the North Atlantic may be linked to tropical cyclones. Su and Smith (2021) have found that tropical cyclones are capable of producing extreme values that influence the upper tail of IVT in these regions. Climate modeling studies have pointed to changes in extratropical transition, a key ingredient of extreme rainfall and water vapor transport, especially for tropical cyclones that pass north of 35° (Haarsma et al. 2013; Baatsen et al. 2015; Ito et al. 2016; Evans et al. 2017; Liu et al. 2017, 2018; Jung and Lackmann 2019; Michaelis and Lackmann 2019) A large region of decreasing trends is found off the coast of California in the Pacific basin, albeit with lower significance level. As California depends heavily on atmospheric rivers (ARs) for its precipitation, the decrease in IVT immediately off its coast reflects the extended period of drought from 2007 to 2016 (see Dettinger et al. 2011, for discussion of the links among ARs, flood, and drought in California).

b. Precipitable water

As with IVT, significant increases are detected in precipitable water across all time scales (Fig. 15). Both the spatial coverage of the 95% significance level and the absolute values of Sen's slope in precipitable water decrease as time scale increases. In contrast to IVT, however, significant increases only cover the

TABLE 6. Maximum n-day IVT and precipitable water W over the box domain of (81°–101°W, 29°–41°N) during the six flood episodes.

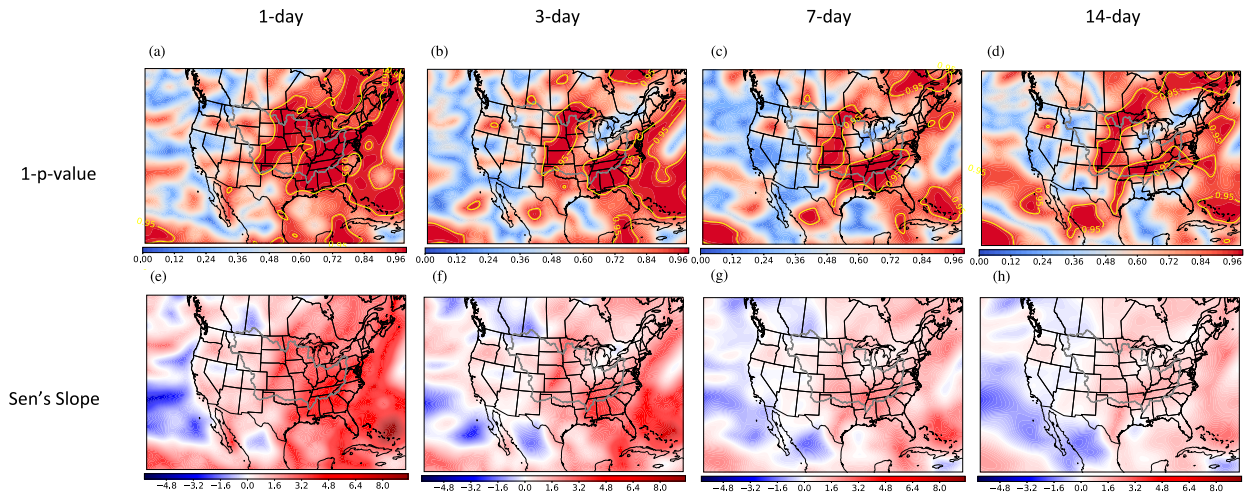|	2008 24 Feb–24 Apr	2011 19 Mar–18 May	2015/16 15 Nov–14 Jan	2017 26 Mar–25 May	2018 15 Jan–16 Mar	2019 13 Jan–14 Mar
1-day IVT	0.99	0.93	0.99	0.98	0.97	0.86
1-day W	0.71	0.99	0.79	0.83	0.75	0.70
3-day IVT	0.88	0.98	1.03	1.09	1.00	0.86
3-day W	0.70	0.74	0.81	0.81	0.68	0.70
7-day IVT	0.72	1.13	1.13	1.00	1.06	1.12
7-day W	0.68	0.69	0.77	0.78	0.69	0.73
14-day IVT	0.74	1.12	1.11	0.91	1.11	1.11
14-day W	0.63	0.63	0.74	0.77	0.68	0.67

FIG. 14. Maps of (a)–(d) significance level and (e)–(h) slope of monotonic trends detected in 1-, 3-, 7-, and 14-day IVT annual maxima time series by the Mann–Kendall test. Yellow lines in (a)–(d) outline regions with greater than 95% significance level. The gray line outlines the Mississippi study domain.

region close to the Vicksburg outlet in the Mississippi domain, at 1- and 3-day time scales. The trend test also detects slight decreases in precipitable water over the upper Missouri River tributary, but the significance level is low, as is the absolute value of the trends. Despite detecting positive trends over most of the domain, the 95% significance level maps (Figs. 15a–d) vary from those of IVT. At the 1- and 3-day time scales, precipitable water is increasing at maximum rates of 0.13 and 0.10 mm yr^{-1} over the Lower Mississippi, respectively.

Trend analyses show that the Mexican Plateau, Gulf Coast, North Atlantic coast, Pacific coast of the northwestern United States, and off the coast of California in the Pacific Ocean experience significant increases in precipitable water extremes across all time scales. Adjacent to the decrease in

upper Missouri, we also observe slight decrease in precipitable water over the semiarid Columbia Plateau, where precipitation depends heavily on the occurrence of atmospheric rivers. The significance level and absolute values of the trends are relatively low. These features are consistent with the trend analyses results in Su and Smith (2021), where they tested 40 years of annual maximum 3-hourly instantaneous precipitable water. Across the four time scales, the variation in the absolute values of the Sen's slope is not as significant in precipitable water (Figs. 15e–h) as it is in IVT (Figs. 14e–h).

c. Precipitable water during maximum IVT

To further understand the main contributor to the increase in IVT over the CONUS, we conduct Mann–Kendall trend
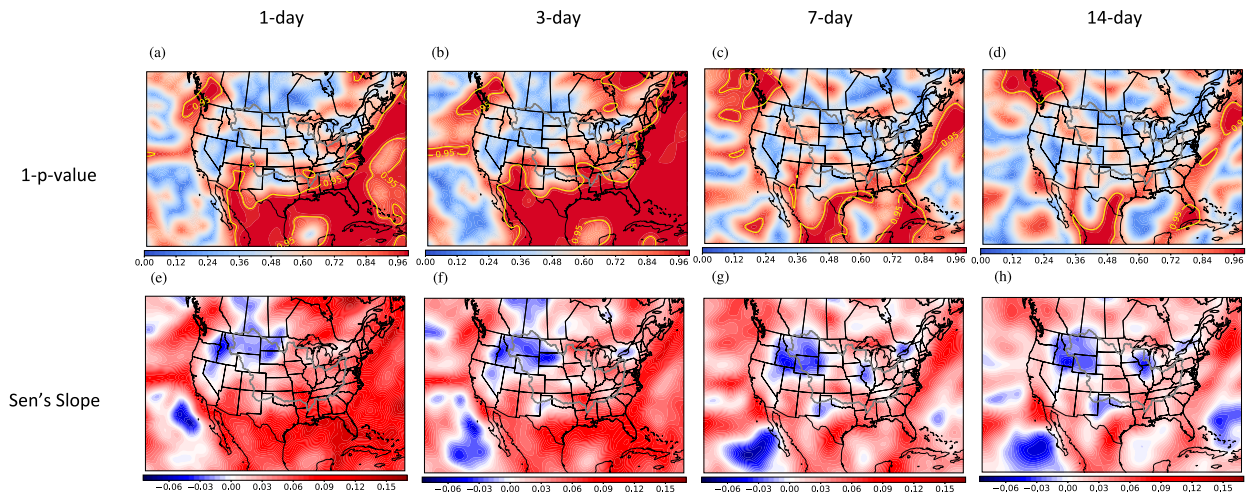

FIG. 15. Maps of (a)–(d) significance level and (e)–(h) slope of monotonic trends detected in 1-, 3-, 7-, and 14-day precipitable water annual maxima time series by the Mann–Kendall test. Yellow lines in (a)–(d) outline regions with greater than 95% significance level. The gray line outlines the Mississippi study domain.
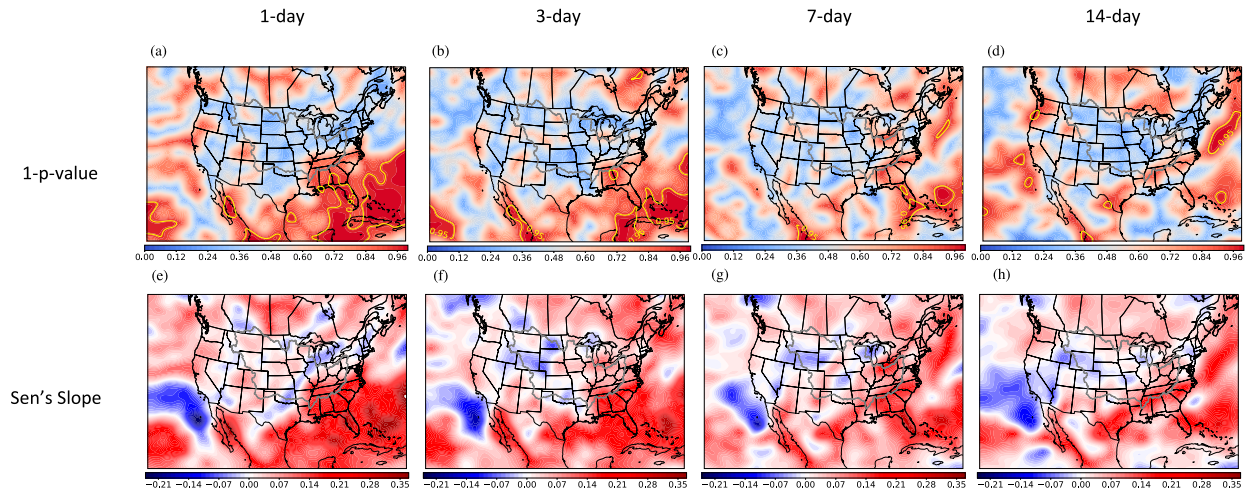
FIG. 16. Maps of (a)–(d) significance level and (e)–(h) slope of monotonic trends detected in 1-, 3-, 7-, and 14-day precipitable water during maximum IVT annual maxima time series by the Mann–Kendall test. Yellow lines in (a)–(d) outline regions with greater than 95% significance level. The gray line outlines the Mississippi study domain.

tests on precipitable water magnitudes during the annual maximum *n*-day IVT time windows (Fig. 16). Results contrast markedly with the IVT trend test results. On the 1- and 3-day time scales, evidence of increase in the moisture content during high transport events is only found in lower latitudes, in the Gulf and North Atlantic basins and over the Florida panhandle. On the 7- and 14-day time scales, the North Atlantic basin off the coast of the northeastern United States exhibits strong evidence for increase. On the 14-day time scale, a region of significant increase is also found over and off the coast of the Columbia River basin. A region of significant decrease is found off the coast of California in the Pacific basin. We detect no significant trends over the Mississippi domain.

Comparison of the non-stationarity results between extremes of IVT (Fig. 14) and extremes of precipitable water during the annual maximum IVT (Fig. 16) suggest that increases in IVT over the continental United States are not principally due to increases in water vapor. Transport is a key factor for trends in IVT extremes. A predictive understanding is needed for changing properties of the size, intensity, and tracks of ARs and extratropical cyclones (e.g., Befort et al. 2016; Wang et al. 2016).

5. Summary and conclusions

Operation of the Bonnet Carré spillway occurred 8 times during the 77-yr period from its completion in 1931–2007. From 2008 to 2020, the flood gates of the spillway have been opened 7 times in 13 years. From once per decade, operation of the spillway has increased to operation every other year. Motivated by the increase in Lower Mississippi River flooding, we investigate the hydrometeorology and hydroclimatology of extreme floods for the largest river in the United States.

The 2 310 000 cfs discharge on 17 May 2011 is the largest on record for the Mississippi River at Vicksburg, eclipsing the

peak from the Great Flood of 1927. The 2011 flood, like the 1927 flood (Smith and Baeck 2015) stands out for the extended period of heavy rainfall over the watershed. A succession of atmospheric rivers passed through the watershed from March to early May; from early March to mid-May, nine distinct AR episodes produced heavy rainfall over the watershed, with the AR beginning on 25 April producing the most extreme rainfall. Each of the six major Lower Mississippi flood episodes was associated with a sequence of ARs.

Also like the 1927 flood, the 2011 flood was characterized by extremes of convective rainfall. The 25–29 April 2011 storms paired extreme rainfall with major tornado outbreaks. Similar combinations of extreme rainfall and severe weather characterized the peak 3-day rainfall periods in December 2015 and April 2017. Storm rotation has received increased attention in connection with extreme rainfall (e.g., Nielsen and Schumacher 2020); clusters of supercells (Knupp et al. 2014) warrant additional study as agents of major flooding in the Lower Mississippi.

The time distribution of rainfall leading to Lower Mississippi River flood peaks exhibits significant variability among the 2008–19 storms. Each includes a dominant 3-day period of extreme rainfall, with most combining multiple episodes of heavy rainfall. Sequencing of storms plays a central role in extreme Lower Mississippi River floods during the period from 2008 to 2019, as recognized by the U.S. Weather Bureau and Corps of Engineers in development of design floods for the Lower Mississippi River (Lott and Myers 1956; Myers 1959). Clustering of ARs may play an important role in Lower Mississippi floods; analyses of West Coast ARs in Fish et al. (2019) provide models for examining sequencing of storm events.

The spatial structure of rainfall for the Lower Mississippi River design storm, "Hypo-Flood 58a" is reflected in rainfall structure for each of the major Lower Mississippi River floods

since 2008. Extreme rainfall is characterized by a southwest–northeast arc of maximum rainfall cutting across the Mississippi Valley. The 3-day rainfall maxima exhibit similarities in rainfall distribution, with rainfall weighted-flow distances clustered around 1100 km. Values of rainfall-weighted flow distance dispersion are also similar for the 3-day rainfall maxima, clustering between 700 and 900 km.

Rainfall structure is dictated by structure and evolution of ARs. Anomaly analyses of IVT and precipitable water during the critical rainfall periods for the six Lower Mississippi flood events reveal southwest to northeast orientation of elevated IVT in the Lower Mississippi Valley. IVT anomalies are markedly larger than precipitable water anomalies. In most events, IVT values during the critical rainfall periods exceed the 10-yr thresholds for large areas of the Mississippi Valley. Precipitable water values, although large for the winter/spring season, never exceed the 10-yr thresholds.

The increased frequency of flooding in the Lower Mississippi River, as reflected in operation of the Bonnet Carré spillway, is paired with significant increases in annual maximum IVT values at time scales ranging from 1 to 14 days, based on Mann–Kendall tests. Significant trends cover the largest spatial area at the 1-day time scale but exist in large portions of the Mississippi domain across all time scales. Extremes in 1-day IVT are increasing over the entire Mississippi domain except for the upper Missouri River region. Extremes in 14-day IVT are observed in two swaths over the Mississippi: a south–north-oriented swath extending from northern Texas to Canada and a southwest–northeast-oriented swath from eastern Texas to the Great Lakes and extending to the east coast. The southwest–northeast swath covers southeastern portions of the Mississippi domain and is closest to the basin outlet. We observe the largest values of increase in this swath.

Significant increases in precipitable water extremes in the Mississippi domain are only found at the 1- and 3-day time scales close to the Mississippi River outlet. There is no significant trend in precipitable water during maximum IVT periods over the domain, implying that changes in transport, and not increases in water vapor, are principal drivers of increases in annual maximum IVT.

The innovative hydrometeorological studies carried out by the U.S. Weather Bureau for design and assessment of the Lower Mississippi flood control system (e.g., Lott and Myers 1956; Myers 1959) have provided the foundation for assessing extreme rainfall and flooding in the largest river of the United States. Climate change and the broader environmental change in the Mississippi River watershed point to the need for renewed assessments of flood defenses for the Lower Mississippi River. Analyses from this study point to important directions in developing new tools for hydrometeorolgoical studies of Lower Mississippi flooding.

From a climatological perspective, sequencing of extreme rainfall from atmospheric rivers is a central ingredient of major flooding in the Lower Mississippi. The distribution of extreme rainfall from an individual AR exhibits characteristic spatial structures that dictate the timing and magnitude of flooding, as reflected in part by the rainfall-weighted flow distance analyses for extreme 3-day rainfall. There is, however,

variability in rainfall magnitudes and additional research is needed to determine the relationships among extreme rainfall, atmospheric water balance components and the storm properties that dictate atmospheric water balance extremes (e.g., Zhang et al. 2019). Clustering of ARs over time periods ranging from weeks to months is also a key ingredient of Lower Mississippi floods. Characterizing clustering of ARs and their associated properties is the key to developing new tools for assessing extreme rainfall and flooding in the Lower Mississippi (see, e.g., Fish et al. 2019, for steps along this path). Time trends in IVT extremes suggest that a predictive understanding is needed for changing properties of ARs, especially size, intensity, and tracks. Trend analyses presented in this study are limited by the 40-yr NARR record; longer datasets will be useful for distinguishing climate change from climate variability (e.g., Munoz and Dee 2017). An atmospheric water balance perspective provides a natural framework for examining the linkages between ARs and extreme rainfall.

REFERENCES

Baatsen, M., R. J. Haarsma, A. J. Van Delden, and H. De Vries, 2015: Severe autumn storms in future Western Europe with a warmer Atlantic Ocean. *Climate Dyn.*, **45**, 949–964, https://doi.org/10.1007/s00382-014-2329-8.

Barry, J. M., 1997: *Rising Tide: The Great Mississippi Flood of 1927 and How it Changed America*. Simon and Schuster, 524 pp.

Befort, D. J., S. Wild, T. Kruschke, U. Ulbrich, and G. C. Leckebusch, 2016: Different long-term trends of extra-tropical cyclones and windstorms in ERA-20C and NOAA-20CR reanalyses. *Atmos. Sci. Lett.*, **17**, 586–595, https://doi.org/10.1002/asl.694.

Bentley, S. J., M. D. Blum, J. Maloney, L. Pond, and R. Paulsell, 2016: The Mississippi River source-to-sink system: Perspectives on tectonic, climatic, and anthropogenic influences, Miocene to Anthropocene. *Earth-Sci. Rev.*, **153**, 139–174, https://doi.org/10.1016/j.earscirev.2015.11.001.

Camillo, C. A., 2012: *Divine Providence: The 2011 Flood in the Mississippi River and Tributaries Project*. Mississippi River Commission, 312 pp.

Chen, J., and P. Kumar, 2002: Role of terrestrial hydrologic memory in modulating ENSO impacts in North America. *J. Climate*, **15**, 3569–3585, https://doi.org/10.1175/1520-0442(2003)015<3569:ROTHMI>2.0.CO;2.

Compo, G. P., J. S. Whitaker, and P. D. Sardeshmukh, 2006: Feasibility of a 100 year reanalysis using only surface pressure data. *Bull. Amer. Meteor. Soc.*, **87**, 175–190, https://doi.org/10.1175/BAMS-87-2-175.

——, and Coauthors, 2011: The twentieth century reanalysis project. *Quart. J. Roy. Meteor. Soc.*, **137**, 1–28, https://doi.org/10.1002/qj.776.

Dettinger, M. D., F. M. Ralph, T. Das, P. J. Neiman, and D. R. Cayan, 2011: Atmospheric Rivers, floods and the water resources of California. *Water*, **3**, 445–478, https://doi.org/10.3390/w3020445.

Dirmeyer, P. A., and J. L. Kinter, 2010: Floods over the U.S. Midwest: A regional water cycle perspective. *J. Hydrometeor.*, **11**, 1172–1181, https://doi.org/10.1175/2010JHM1196.1.

Du, J., 2011: NCEP/EMC 4KM Gridded Data (GRIB) Stage IV data, version 1.0. UCAR/NCAR–Earth Observing Laboratory, accessed 16 December 2022, https://doi.org/10.5065/D6PG1QDD.

Evans, C., and Coauthors, 2017: The extratropical transition of tropical cyclones. Part I: Cyclone evolution and direct impacts. *Mon. Wea. Rev.*, **145**, 4317–4344, https://doi.org/10.1175/MWR-D-17-0027.1.

Fish, M. A., A. M. Wilson, and F. M. Ralph, 2019: Atmospheric river families: Definition and associated synoptic conditions. *J. Hydrometeor.*, **20**, 2091–2108, https://doi.org/10.1175/JHM-D-18-0217.1.

——, J. M. Done, D. L. Swain, A. M. Wilson, A. C. Michaelis, P. B. Gibson, and F. M. Ralph, 2022: Large-scale environments of successive atmospheric river events leading to compound precipitation extremes in California. *J. Climate*, **35**, 1515–1536, https://doi.org/10.1175/JCLI-D-21-0168.1.

Haarsma, R. J., W. Hazeleger, C. Severijns, H. De Vries, A. Sterl, R. Bintanja, G. J. Van Oldenborgh, and H. W. Van Den Brink, 2013: More hurricanes to hit Western Europe due to global warming. *Geophys. Res. Lett.*, **40**, 1783–1788, https://doi.org/10.1002/grl.50360.

Hart, R. E., and R. H. Grumm, 2001: Using normalized climatological anomalies to rank synoptic-scale events. *Mon. Wea. Rev.*, **129**, 2426–2442, https://doi.org/10.1175/1520-0493(2001)129<2426:UNCATR>2.0.CO;2.

Helsel, D. R., and R. M. Hirsch, 1993: *Statistical Methods in Water Resources*. Elsevier, 522 pp.

Ito, R., T. Takemi, and O. Arakawa, 2016: A possible reduction in the severity of typhoon wind in the northern part of Japan under global warming: A case study. *SOLA*, **12**, 100–105, https://doi.org/10.2151/sola.2016-023.

Jennrich, G. C., J. C. Furtado, J. B. Basara, and E. R. Martin, 2020: Synoptic characteristics of 14-day extreme precipitation events across the United States. *J. Climate*, **33**, 6423–6440, https://doi.org/10.1175/JCLI-D-19-0563.1.

Jung, C., and G. M. Lackmann, 2019: Extratropical transition of Hurricane Irene (2011) in a changing climate. *J. Climate*, **32**, 4847–4871, https://doi.org/10.1175/JCLI-D-18-0558.1.

Knupp, K. R., and Coauthors, 2014: Meteorological overview of the devastating 27 April 2011 tornado outbreak. *Bull. Amer.*

Meteor. Soc., **95**, 1041–1062, https://doi.org/10.1175/BAMS-D-11-00229.1.

Kunkel, K. E., T. R. Karl, M. F. Squires, X. Yin, S. T. Stegall, and D. R. Easterling, 2020a: Precipitation extremes: Trends and relationships with average precipitation and precipitable water in the contiguous United States. *J. Appl. Meteor. Climatol.*, **59**, 125–142, https://doi.org/10.1175/JAMC-D-19-0185.1.

——, S. E. Stevens, L. E. Stevens, and T. R. Karl, 2020b: Observed climatological relationships of extreme daily precipitation events with precipitable water and vertical velocity in the contiguous United States. *Geophys. Res. Lett.*, **47**, e2019GL086721, https://doi.org/10.1029/2019GL086721.

Lavers, D. A., and G. Villarini, 2013: Atmospheric Rivers and flooding over the central United States. *J. Climate*, **26**, 7829–7836, https://doi.org/10.1175/JCLI-D-13-00212.1.

Lehner, B., K. Verdin, and A. Jarvis, 2008: New global hydrography derived from spaceborne elevation. *Eos, Trans. Amer. Geophys. Union*, **89**, 93–94, https://doi.org/10.1029/2008EO100001.

Lin, Y., and K. E. Mitchell, 2005: The NCEP Stage II/IV hourly precipitation analyses: Development and applications. *19th Conf. on Hydrology*, San Diego, CA, Amer. Meteor. Soc., 1.2, https://ams.confex.com/ams/Annual2005/techprogram/paper_83847.htm.

Liu, M., G. A. Vecchi, J. A. Smith, and H. Murakami, 2017: The present-day simulation and twenty-first-century projection of the climatology of extratropical transition in the North Atlantic. *J. Climate*, **30**, 2739–2756, https://doi.org/10.1175/JCLI-D-16-0352.1.

——, ——, ——, and ——, 2018: Projection of landfalling–tropical cyclone rainfall in the eastern United States under anthropogenic warming. *J. Climate*, **31**, 7269–7286, https://doi.org/10.1175/JCLI-D-17-0747.1.

Lott, G. A., and V. A. Myers, 1956: Meteorology of flood-producing storms in the Mississippi River basin. Weather Bureau Hydrometeorological Rep. 34, 226 pp.

Mahoney, K., and Coauthors, 2016: Understanding the role of atmospheric rivers in heavy precipitation in the southeast United States. *Mon. Wea. Rev.*, **144**, 1617–1632, https://doi.org/10.1175/MWR-D-15-0279.1.

Mesinger, F., and Coauthors, 2006: North American regional reanalysis. *Bull. Amer. Meteor. Soc.*, **87**, 343–360, https://doi.org/10.1175/BAMS-87-3-343.

Michaelis, A. C., and G. M. Lackmann, 2019: Climatological changes in the extratropical transition of tropical cyclones in high-resolution global simulations. *J. Climate*, **32**, 8733–8753, https://doi.org/10.1175/JCLI-D-19-0259.1.

Moore, B. J., P. J. Neiman, F. M. Ralph, and F. E. Barthold, 2012: Physical processes associated with heavy flooding rainfall in Nashville, Tennessee, and vicinity during 1–2 May 2010: The role of an atmospheric river and mesoscale convective systems. *Mon. Wea. Rev.*, **140**, 358–378, https://doi.org/10.1175/MWR-D-11-00126.1.

——, K. M. Mahoney, E. M. Sukovich, R. Cifelli, and T. M. Cahill, 2015: Climatology and environmental characteristics of extreme precipitation events in the Southeastern United States. *Mon. Wea. Rev.*, **143**, 718–741, https://doi.org/10.1175/MWR-D-14-00065.1.

Munoz, S. E., and S. G. Dee, 2017: El Niño increases the risk of lower Mississippi River flooding. *Sci. Rep.*, **7**, 1772, https://doi.org/10.1038/s41598-017-01919-6.

——, and Coauthors, 2018: Climatic control of Mississippi River flood hazard amplified by river engineering. *Nature*, **556**, 95–98, https://doi.org/10.1038/nature26145.

Myers, V. A., 1959: Meteorology of hypothetical flood sequences in the Mississippi River basin. Weather Bureau Hydrometeorological Rep. 35, 45 pp.

Nayak, M. A., and G. Villarini, 2017: A long-term perspective of the hydroclimatological impacts of atmospheric rivers over the central United States. *Water Resour. Res.*, **53**, 1144–1166, https://doi.org/10.1002/2016WR019033.

Neiman, P. J., F. M. Ralph, G. A. Wick, J. D. Lundquist, and M. D. Dettinger, 2008: Meteorological characteristics and overland precipitation impacts of atmospheric rivers affecting the West Coast of North America based on eight years of SSM/I satellite observations. *J. Hydrometeor.*, **9**, 22–47, https://doi.org/10.1175/2007JHM855.1.

Newell, R. E., N. E. Newell, and Y. Zhu, 1992: Tropospheric Rivers? A pilot study. *Geophys. Res. Lett.*, **19**, 2401–2404, https://doi.org/10.1029/92GL02916.

Nielsen, E. R., and R. S. Schumacher, 2020: Observations of extreme short-term precipitation associated with supercells and mesovortices. *Mon. Wea. Rev.*, **148**, 159–182, https://doi.org/10.1175/MWR-D-19-0146.1.

Pohlert, T., 2018: Non-parametric trend tests and change-point detection, version 1.1.1. R package, https://CRAN.R-project.org/package=trend.

Ralph, F. M., P. J. Neiman, G. A. Wick, S. I. Gutman, M. D. Dettinger, D. R. Cayan, and A. B. White, 2006: Flooding on California's Russian River: Role of atmospheric rivers. *Geophys. Res. Lett.*, **33**, L13801, https://doi.org/10.1029/2006GL026689.

——, and Coauthors, 2019: A scale to characterize the strength and impact of atmospheric rivers. *Bull. Amer. Meteor. Soc.*, **100**, 269–289, https://doi.org/10.1175/BAMS-D-18-0023.1.

Russell, C., C. N. Waters, S. Himson, R. Holmes, A. Burns, J. Zalasiewicz, and M. Williams, 2021: Geological evolution of the Mississippi River into the anthropocene. *Anthropocene Rev.*, **8**, 115–140, https://doi.org/10.1177/20530196211045527.

Slivinski, L. C., and Coauthors, 2019: Towards a more reliable historical reanalysis: Improvements for version 3 of the Twentieth Century Reanalysis system. *Quart. J. Roy. Meteor. Soc.*, **145**, 2876–2908, https://doi.org/10.1002/qj.3598.

Smith, J. A., and M. L. Baeck, 2015: "Prophetic vision, vivid imagination": The 1927 Mississippi River flood. *Water Resour. Res.*, **51**, 9964–9994, https://doi.org/10.1002/2015WR017927.

——, ——, Y. Zhang, and C. A. Doswell III, 2001: Extreme rainfall and flooding from supercell thunderstorms. *J. Hydrometeor.*, **2**, 469–489, https://doi.org/10.1175/1525-7541(2001)002<0469:ERAFFS>2.0.CO;2.

——, ——, J. E. Morrison, P. Sturdevant-Rees, D. F. Turner-Gillespie, and P. D. Bates, 2002: The regional hydrology of extreme floods in an urbanizing drainage basin. *J. Hydrometeor.*, **3**, 267–282, https://doi.org/10.1175/1525-7541(2002)003<0267:TRHOEF>2.0.CO;2.

——, ——, K. L. Meierdiercks, P. A. Nelson, A. J. Miller, and E. J. Holland, 2005: Field studies of the storm event hydrologic response in an urbanizing watershed. *Water Resour. Res.*, **41**, W10413, https://doi.org/10.1029/2004WR003712.

Steiner, M., and J. A. Smith, 1998: Convective versus stratiform rainfall: An ice-microphysical and kinematic conceptual model. *Atmos. Res.*, **47–48**, 317–326, https://doi.org/10.1016/S0169-8095(97)00086-0.

Su, Y., and J. A. Smith, 2021: An atmospheric water balance perspective on extreme rainfall potential for the contiguous US. *Water Resour. Res.*, **57**, e2020WR028387, https://doi.org/10.1029/2020WR028387.

Van der Wiel, K., S. B. Kapnick, G. A. Vecchi, J. A. Smith, P. C. Milly, and L. Jia, 2018: 100-year lower Mississippi floods in a global climate model: Characteristics and future changes. *J. Hydrometeor.*, **19**, 1547–1563, https://doi.org/10.1175/JHM-D-18-0018.1.

Virtanen, P., and Coauthors, 2020: SciPy 1.0: Fundamental algorithms for scientific computing in Python. *Nat. Methods*, **17**, 261–272, https://doi.org/10.1038/s41592-019-0686-2.

Wang, X. L., Y. Feng, R. Chan, and V. Isaac, 2016: Intercomparison of extra-tropical cyclone activity in nine reanalysis datasets. *Atmos. Res.*, **181**, 133–153, https://doi.org/10.1016/j.atmosres.2016.06.010.

Wiman, C., B. Hamilton, S. G. Dee, and S. E. Muñoz, 2021: Reduced lower Mississippi River discharge during the Medieval era. *Geophys. Res. Lett.*, **48**, e2020GL091182, https://doi.org/10.1029/2020GL091182.

World Meteorological Organization, 2009: Manual on estimation of probable maximum precipitation (PMP). Tech. Rep. WMO-1045, 257 pp.

Wu, C.-Y., J. Mossa, and J. M. Jaeger, 2022: Estimate of decadal-scale riverbed deformation and bed-load sediment transport during flood events in the lowermost Mississippi River. *Earth Surf. Processes Landforms*, **47**, 1271–1286, https://doi.org/10.1002/esp.5316.

Zhang, Z., F. M. Ralph, and M. Zheng, 2019: The relationship between extratropical cyclone strength and atmospheric river intensity and position. *Geophys. Res. Lett.*, **46**, 1814–1823, https://doi.org/10.1029/2018GL079071.

Zhu, Y., and R. E. Newell, 1998: A proposed algorithm for moisture fluxes from atmospheric rivers. *Mon. Wea. Rev.*, **126**, 725–735, https://doi.org/10.1175/1520-0493(1998)126<0725:APAFMF>2.0.CO;2.